LAWRENCE
LIVERMORE
NATIONAL
LABORATORY

UCRL-JRNL-219543

Size and habit evolution of PETN crystals - a lattice Monte Carlo study

Luis A. Zepeda-Ruiz, Amitesh Maiti, Richard Gee, George H. Gilmer, Brandon Weeks

March 6, 2006

Journal of Crystal Growth

Size and habit evolution of PETN crystals – a lattice Monte Carlo study

Luis A. Zepeda-Ruiz,[1] Amitesh Maiti,[1] Richard Gee,[1] George H. Gilmer[1], and Brandon Weeks[2]

[1]Lawrence Livermore National Laboratory, Livermore, CA 94550

[2]Department of Chemical Engineering, Texas Tech University, Lubbock, TX 79409-3121

Abstract

Starting from an accurate inter-atomic potential we develop a simple scheme of generating an "on-lattice" *molecular* potential of short range, which is then incorporated into a lattice Monte Carlo code for simulating size and shape evolution of nanocrystallites. As a specific example, we test such a procedure on the morphological evolution of a molecular crystal of interest to us, e.g., Pentaerythritol Tetranitrate, or PETN, and obtain realistic facetted structures in excellent agreement with experimental morphologies. We investigate several interesting effects including, the evolution of the initial shape of a "seed" to an equilibrium configuration, and the variation of growth morphology as a function of the rate of particle addition relative to diffusion.

1. Introduction

PETN (Pentaerythritol Tetranitrate) is a commonly used explosive for both military and civilian applications. It is one of the simplest mono-energetics containing both fuel and oxidizer in the same molecule. One important factor in the energetic properties of the high explosives is its density, whose value depends on the overall crystal morphology. It is well known that at or near the theoretical maximum density of an energetic material it is difficult, if not impossible to induce a detonation. Further, the decomposition rate within a material is not simply an intrinsic property of the explosive such as the chemical composition. Rather, it is determined by a number of factors including the particle characteristics of the explosive including morphology and surface area. Therefore, it is important to be able to predict the habit and shape of explosives crystals and understand the increase in average crystallite size, which may change the overall density of the explosive.

The size and shape distribution of crystallites controls important materials properties, such as chemical, mechanical, thermal, and optical properties that can be quite different from the bulk. It is therefore not surprising that many studies exist in the literature, both experimental and theoretical, of how crystallites grow and change shape and how such evolution is affected by external factors like stress, temperature, solvent, additives and so on [1, 2]. General theories for predicting crystal morphology based on considerations of geometry [3, 4], surface free energy [5], and attachment energy [6-8] have been around for several decades. Using empirical inter-atomic potentials such theories have been used to predict the "average" morphology of crystallites belonging to a wide variety of materials types: metallic, semiconductors, ionic, organic, etc. However, such approaches yield morphologies where kinetics are included only in a very approximate way. Real systems typically consist of a distribution of crystallite shapes and

sizes. For an understanding of how such a distribution depends on various external factors, it is desirable to create a simulation method that takes important kinetic processes into account, such as the ratio between diffusion and incorporation of molecules.

Although inorganic crystallization has been studied in detail over the past few decades, investigations of organic (or molecular crystals) using atomistic simulations have begun somewhat recently [9, 10]. With additional complexity stemming from a molecule's internal degrees of freedom, the major focus so far has been designing Monte Carlo algorithms to predict packing arrangements within the crystal. There has been insightful work on the average morphology prediction using the Hartman-Perdok (HP) theory and its extensions [11, 12], as well as phenomenological studies of crystallite distribution using classical nucleation theory [13]. However, we are not aware of any materials-specific work related to direct growth/dissolution simulations of an ensemble of crystallites. While classical molecular dynamics (MD) simulations could provide useful insight into basic atomistic processes, it is limited by several orders of magnitude in time in its ability to simulate most crystal growth techniques, except for fast processes like rapid solidification and pulsed laser deposition. Thus, one would typically take recourse to a kinetic Monte Carlo (KMC) scheme. Over the last couple of decades several KMC codes have been devised primarily with the aim of simulating the growth of inorganic thin films [14-16]. Adapting such codes to organic crystallites is possible, but would require modifications.

We report here a simple lattice Monte Carlo scheme where whole molecules are treated as the basic entities. This allows replacing complex inter-atomic potentials with a simple potential describing molecule-molecule interactions, which is defined on grid-points of the molecular lattice. For molecules like PETN with no *net* charge or dipole moment, this potential is expected

to be of short range, and therefore one would expect to neglect molecule-molecule interactions after only a few nearest neighbors. The resulting fast computation of potential energy allows for simulations with large crystallites over long simulation times, and enables investigations of a number of interesting effects in a reasonable amount of time.

2. Experiments on PETN

A typical PETN crystal is shown in Fig. 1(a). Although this crystal was grown from solution, it exhibits the primary facets that are observed during growth from the vapor. This crystal was grown by slow recrystallization from acetone yielding colorless crystals at 4^{o}C and have an average aspect ratio of 5:2 for the length:width. Figure 1(b) shows the predicted growth morphology or crystal "habit" of a PETN crystal obtained by a standard Wulff construction but using the so-called attachment energies instead of surface free energies [6]. Table 1 lists the attachment and surface energies (per unit area) for the most stable faces of the PETN crystal. The method used in the calculation of these values is discussed in the next section. A Wulff construction based on the surface free energies yields the equilibrium morphology, which for the PETN crystal looks very similar to the growth morphology of Fig. 1(b) and therefore is not shown. In the computed morphology, the crystal habit matches the experimentally grown crystal of Fig. 1(a), where four {110} facets are shown along the length (long axis), while the end caps are facetted by eight planes belonging to the {101} family. However, most of the experimental particles deviate from the nice symmetry of Fig. 1(b).

These solution grown crystals are compressed to 50% of its theoretical maximum density and the resulting powder is stored for several years. At room temperature the powder is stable

showing no rearrangement over a period of several days. Because PETN molecules have a relatively high surface mobility, the morphology and surface area change over time due to surface diffusion and/or sublimation/recrystallization. The rate of recrystallization and the aspect ratio of the crystallites are strongly dependent on the temperature at which the PETN is kept. The change in aspect ratio may result by changing the supersaturation of the environment where the PETN powder is maintained. Although the particle size distribution can be measured experimentally, there is little information on the mechanism associated with the change in surface area. The resulting morphology during aging also appears to be dominated by the two families of facets shown in Fig. 1(b). Figure 1(c) is a SEM micrograph of PETN crystallites resulting from subliming PETN powder followed by aging at 80 ^{o}C for 90 days at ambient pressure. These crystallites in Fig. 1(c) show a clear propensity for elongation along the <001> axis, with aspect ratio in excess of 100:3 for some of the crystallites. Although crystallites are elongated along the crystal <001> axis, the ratios of surface area of the {110} to the {101} facets vary significantly from crystallite to crystallite and the areas of the end {101} faces are typically unequal within the same crystallite.

3. Lattice potential

Figures 2(a) and (b) respectively display the equilibrium structure of a PETN molecule optimized by the COMPASS forcefield [17, 18], and the experimental crystal structure of PETN [19]. The H-atom positions in the experimental crystal structure, which cannot be easily deciphered from X-ray crystal data, were optimized by COMPASS as well. The lattice energy (normalized per molecule) E_{Lat} of this structure is computed as -38.8 kcal/mol, which agrees quite well with an experimental value of -36.3 kcal/mol [20, 21].

As a prelude to MC simulations we carried out several classical MD simulations on both {110} and {101} facets. We found that if we add an extra PETN molecule at an arbitrary orientation to a surface cleaved from the experimental bulk structure, the molecule quickly snaps into the nearest lattice position in the same orientation as a PETN molecule in the crystal lattice. This provided justification that one could consider a molecule as a basic entity and use an effective molecule-molecule interaction potential defined from the bulk lattice. Furthermore, since a PETN molecule does not carry a net charge or a dipole moment, it is reasonable to assume that such a potential would fall off fast enough, so that one could justifiably limit energy computation to only the first few neighbors. To quantify the rate of this fall-off, we note that the lattice energy can be written as a sum of such a potential over all neighbor shells, i.e.,

$$E_{Lat} = \frac{1}{2}\sum_{i=1}^{\infty} Z_i E_{MM}(i) + \Delta E ,$$

where $E_{MM}(i)$ is the molecular interaction energy between i^{th} neighbors [22] (i.e. neighbors belonging to the i^{th} shell), Z_i is the number of i^{th} shell neighbors, and ΔE is a positive number denoting the energy of relaxation of an isolated molecule (i.e., in the gas phase) from its structure in the bulk lattice, with a value of 4.46 kcal/mol, computed using COMPASS. It is therefore desired that not only $E_{MM}(i)$ fall off fast with i, but so does the difference of the total E_{Lat} from the cumulative contribution to E_{Lat} due to all neighbors on and within the i^{th} shell, given by

$$E_{cum}(i) = \frac{1}{2}\sum_{j=1}^{i} Z_j E_{MM}(j) + \Delta E .$$

Table 2 displays such an interaction potential (E_{MM}) and E_{cum} for the first five neighbors, and shows that it would be good approximation to cut off the potential beyond the fourth or fifth nearest neighbor.

4. MC Simulation Method

As mentioned before, we substitute the entire PETN molecule, $C(CH_2ONO_2)_4$, by a single unit whose interaction depends on its local environment, i.e., number and type of neighbors, as shown in Fig. 3. This allows us to substitute the complexity of the 29 atoms that form a PETN molecule by an equivalent unit that is packed on a body center tetragonal lattice, and to study the unit-unit interaction on a lattice in a manner similar to crystal graph theory of Hartman-Perdok [6]. These new PETN units interact according to the values given in Table 2. Starting from a given initial configuration, each MC step consists of choosing a particle at random and moving it to a randomly chosen unoccupied site within a given cutoff radius. Next, we calculate the change of energy, ΔE, due to this move. The new configuration is accepted with probability 1 if the resulting energy change ΔE is less than zero, and accepted with a probability $\exp(-\Delta E/k_BT)$ otherwise. This *local* random walk can be interpreted as the result of a few successive neighboring hops. Such procedure ensures that all possible configurations can be sampled. Also since all attempted atomic displacement steps obey detail balance it implies that the system approaches an equilibrium configuration as the simulation time approaches infinity. A more accurate simulation of the kinetics of the morphology evolution would involve neighboring diffusional steps weighted by factors determined by the activation barriers and changes in energy. This would require the calculation of a large number of possible diffusion pathways, the corresponding transition states, and hopping rates.

The experimental conditions of relevance here are such that PETN crystallites evolve from a supersaturated vapor phase through nucleation and growth. Therefore, our kMC model includes only two events, surface diffusion hops and addition of new molecules to the crystal. The reconfiguration must be caused by molecular diffusion across the surface of each crystallite and diffusion between crystals that are in contact, or that share a contact with a third crystal. Since the starting configuration of the PETN for the experiments is a finely divided powder, there is a tendency for molecules that are on sites with few interacting neighbors to diffuse across the surface to more favorable positions. It is this process that we simulate by adding molecules at the surface.

The nanometer length scale of the crystallites that will be obtained with our MC model is much smaller than that shown in the micrographs. In order to reach the micron size, we would require simulation systems of size $\sim 10^9$ or more molecules which are beyond our current computational capabilities. In the equilibrium limit the shapes of the crystallites on all length scales are self-similar. However, there are size-dependent effects on the growth morphologies, which can be qualitatively explored through nanoscale simulations, such as those presented in this paper.

5. MC Results

The influence of crystallographic anisotropy on the growth and evolution of PETN crystals is most clearly observed in the case of a full three-dimensional system in which all crystallographic orientations are accessible for diffusive transport. As a first step in our analysis of size and habit evolution, we decided to study the evolution of the shape of a PETN crystal starting from an

arbitrary initial shape. Fig. 4(a) displays the specific example of a *spherical* crystallite of diameter 16 nm, which was equilibrated for $2x10^6$ MC steps. The reason for choosing a sphere was to eliminate any directional bias or artificial anisotropy that might influence the resulting crystallite shape. The resulting configuration, Fig. 4(b) shows the presence of {101} and {110} facets, also present in the Hartman-Perdok predicted morphology of Fig. 1(b). In addition, four small {100} faces are also present. Note the comparable surface energies (obtained by COMPASS calculations) between these 3 faces: 0.21, 0.27 and 0.27 kcal/(mol.Å^2) for the {101}, {110}, and {100} surface, respectively. Thus, the appearance of these facets in the equilibrated structure gave us confidence not only in the accuracy of the inter-molecular lattice potential, but also its ability to mimic realistic crystallite shapes when used with the MC procedure described above.

The morphology in Fig. 4(b) results from the "local rearrangement" of a fixed number of particles (the ones that formed the initial spherical crystallite) driven by the tendency of the system energy to reach a local minimum. However, the experimentally observed morphologies are a result of growth through particle addition and diffusion, whose rates strongly depend on experimental conditions. To this end, we have studied the change in morphology during growth in a similar way as described in Ref. [14]. Thus, we start from an initial spherical seed, and add particles to the surface of the growing crystallite along a randomly selected radial direction [14]. Following each particle addition we perform a pre-defined number of MC steps, aimed at representing surface diffusion. Thus the above number of MC steps between two successive particle addition events represents, on an average, the ratio of the diffusion hop rate to the crystallite growth rate.

Figure 5 shows the evolution of an initial spherical seed of 5 nm in diameter at 300 K. We performed 17 MC steps per insertion and particles were allowed to move within a cutoff radius of 5 nm. After insertion of only 200 particles, as shown in Fig 5(b), the surface of the crystal is bounded by {101} and {110} facets of approximately the same size. As more material is added to the crystal, {110} facets become dominant as shown in Fig. 5(c). This is a result of the difference in adatom potential energy between these two faces. The {101} faces have a lower adatom potential energy (-28.7 kcal/mol) than the {110} faces (-18.7 kcal/mol), thus making the nucleation of a new layer easier and leading to a faster growth, as shown in Fig. 5(d). As the crystal grows larger, the {110} facets can nucleate stable two dimensional islands that allow these faces to grow through the motion of monatomic steps, as shown in Fig. 5(e).

Controlling the ratio between the sizes of the {101} and {110} facets can be achieved by varying experimental conditions such as deposition rate and growth temperature. Experimental data suggest that at lower temperatures crystallites tend to be more round with a {110}/{101} aspect ratio being close to unity, while elevated temperatures tend to yield needle-like crystals as those shown in Fig. 1(c). Temperature clearly affects all the important kinetic processes, i.e., adsorption, desorption, and diffusion rates on each surface. Although we eventually plan on computing and implementing the important rates into our MC, as a first approximation we decided to incorporate the temperature effects simply by varying the number of MC steps between insertions of new particles. Figures 6(a-e) shows the resulting configurations following 3.5×10^4 particle insertions respectively at the rates of 5, 10, 25, 50 and 100 MC diffusion steps between insertions. This variation can be interpreted either as an increase in surface diffusivity (e.g., by increasing the growth temperature) or as a decrease in growth rate. Therefore the progressively needle-like evolution in going from Fig. 6(a) to 6(e) is a clear manifestation of

what is seen experimentally (Fig. 1(c)). It is apparent that the results shown in Fig. 6 have little relationship to the equilibrium shape of the crystal shown in Fig. 4(b). To explain the long needle-like shapes based on equilibrium morphologies would require large ratios between the surface free energies; ratios corresponding to the aspect ratios of the crystal shapes. The wide variation in morphologies observed in real crystals of PETN is direct evidence of the predominance of kinetics in this system, even though these crystals are not formed under highly non-equilibrium conditions.

The change in the morphology from the rounded shapes at low temperatures (few diffusion hops) to the anisotropic shapes at high temperatures can also be understood in terms of the surface diffusion occurring between molecule additions. If a molecule makes only a few diffusion hops before another molecule arrives in its vicinity, then nucleation is favored by the high probability of the association of the two molecules into a small cluster. The high nucleation probability means that molecules are likely to stick close to the point where they originate, and the various crystal faces will advance at approximately the same rate. At high temperatures where the molecules execute a large number of diffusion hops between molecule additions, they diffuse over larger distances as a mobile unit before joining a surface cluster or encountering another molecule to form a new cluster. Some of the molecules will be able to diffuse across the surface of the crystallite to another facet. The exchange of molecules between facets will result in higher concentrations of mobile species on the facets where the potential energy is lower, and this will in turn result in a disparity in growth rates on the facets. Thus, the higher diffusion rates at high temperature result in large variations in the growth rates as a consequence of different rates of the nucleation of clusters on the faces. Equilibrium forms based on Wulf

plots, where the anisotropies in surface free energies cause only a relative small variation in the facet sizes, cannot explain this kinetic effect.

6. Summary and future work

Using a simple, yet accurate inter-molecular lattice potential in conjunction with the described MC scheme we have studied the morphological evolution of a realistic molecular crystallite (PETN). Our simulations reproduce all the experimentally observed facets, and show that the overall shapes strongly depend on the relative rates of particle addition and diffusion. The success of atomistic models such as the one presented here is encouraging, and shows that the inclusion of basic mechanisms such as surface diffusion and two-dimensional nucleation is sufficient to explain these disparate morphologies. Even at small driving forces, the two-dimensional nucleation rate can vary over many orders of magnitude on different facets of the same crystal. Since crystal morphologies are crucial for many industrial applications, the ability to choose conditions to produce the desired structures is essential. Appropriate models for these processes are needed in a variety of fields, including the exciting area of self-assembling nanostructures, energetic materials, etc. Finally, the methodology presented here is general, and the code in its present form can be readily extended to more complex problems, e.g., the study of size and shape evolution of a distribution of crystallites, or the modification of crystallite morphology by designer additives and changing temperatures. Some of that work is currently underway.

Acknowledgment

This work was performed under the auspices of the U.S. Department of Energy by the University of California, Lawrence Livermore National Laboratory under Contract No. W-7405-Eng-48. Support from the Basic Energy Sciences office of the Department of Energy is also acknowledged. We would like to thank Melissa Moore and Arnie Duncan of the Applied Technology division of BWXT Pantex for stimulating discussions and for permission to use the experimental image Fig. 1(c).

References:

1. J. W. Mullin, *Crystallization*, 4th Ed., Butterworth-Heinemann Ltd. (2001).
2. H. J. Scheel and T. Fukuda, *Crystal Growth Technology*, Wiley (2003).
3. A. Bravais, Etudes Crystallographiques, Acedemie des Sciences, Paris (1913)
4. J. D. H. Donnay, D. Harker, Amer. Mineralogist 22 (1937) 463.
5. J. W. Gibbs, Collected Works, Longman, New York (1928).
6. P. Hartman, W. G. Perdok, Acta Cryst. 8 (1955) 49.
7. R. Docherty, et al. J. Phys. D **24**, (1991) 89-99
8. M. Brumsteiner and S. L. Price, Cryst. Growth & Design **1**, (2001) 447-453.
9. Z. Berkovitch-Yellin, J. Am. Chem. Soc. 107 (1985) 8239.
10. A. S. Myerson, D. A. Green, Paul Meenan (eds.) *Crystal Growth of Organic Materials*, ACS Publications (1996).
11. A. S. Myerson (ed.) *Molecular Modeling Applications in Crystallization*, Cambridge University Press (1999).
12. P. Bennema, J. Cryst. Growth 166 (1996) 17.
13. J. A. Dirksen, T. A. Ring, Chem. Eng. Sci. 46 (1991) 2389.
14. H. Huang, G. H. Gilmer, T. Diaz de la Rubia, J. Appl. Phys. 84 (1998) 3636.
15. D. H. Gay, A. L. Rohl, J. Chem. Soc. Faraday Trans. 91 (1995) 925.
16. S. X. M. Boerrigter et al., J. Phys. Chem. A **108**, (2004) 5894-5902.

17. H. Sun, J. Phys. Chem. B 102 (1998) 7338.

18. S. W. Bunte and H. Sun, J. Phys. Chem. B **104** (2000) 2477.

19. J. Trotter, Acta Crysta 16 (1963) 698.

20. J. S. Chickos, Heats of sublimation, in: J. F. Liebman, A. Greenberg (eds.), Molecular Structure and Energetics, VCH Publishers, New York, 1987, chapter 2.

21. G. Edwards, Trans. Faraday Soc. 49 (1953) 152.

22. Note that the quantity $E_{MM}(i)$ is computed using the COMPASS forcefield [17, 18], which includes explicit charges on all atoms. Therefore, it includes electrostatic as well as van der Waals contributions. However, the net charge and the net dipole moment of each PETN molecule is zero, which leads to a rapid fall-off of $E_{MM}(i)$ with neighbor distance.

Table 1: Surface and attachment energies for some of the most stable faces of PETN crystal computed using the COMPASS forcefield [17, 18]. The surface energies are used to construct the equilibrium morphology, while the attachment energies are used to construct the growth morphology.

Surface (Miller Index)	Surface Energy (kcal/mol.Å^2)	Attachment Energy (kcal/mol)
{101}	0.21	-36.8
{110}	0.27	-56.9
{100}	0.27	-63.2
{210}	0.26	-51.8
{201}	0.30	-71.1
{211}	0.28	-70.9

Table 2: Molecule-molecule interaction potential (E_{MM}) as defined for the first five nearest neighbors. The potential is computed by the COMPASS forcefield [17, 18]. The last column (E_{cum}) indicates the cumulative contribution to cohesive energy due to all E_{MM} within the given neighbor distance, and displays a smooth saturation toward the bulk lattice energy E_{Lat} = -38.8 kcal/mol. Experimental lattice energy is -36.3 kcal/mol.

Neighbor shell # (i)	Neighbor lattice index	Neighbor distance (Å)	# Neighbors (Z_i)	$E_{MM}(i)$ (kcal/mol)	$E_{cum}(i)$ (kcal/mol)
1	0 0 1	6.71	2	-9.86	-5.4
2	½ ½ ½	7.43	8	-6.81	-32.6
3	1 0 0	9.38	4	-0.47	-33.5
4	0 1 1	11.53	8	-0.59	-35.9
5	½ ½ 1½	12.05	8	-0.47	-37.8

Figure Captions:

Figure 1. (a) Microscope image of a typical PETN crystal grown from solution. (b) Hartman-Perdok (HP) growth morphology of PETN as computed by the COMPASS forcefield via the attachment energy method. Two types of facets are prominent, four elongated faces of the {110} family and eight end faces of the {101} family. (c) Microscope image of typical PETN crystallites illustrating a variety of aspect ratios after aging.

Figure 2. (a) PETN molecule optimized by COMPASS. (b) experimental crystal structure of PETN with positions of H atoms optimized by COMPASS. Color scheme: C (grey), O (red), N (blue), and H (white). The experimental structure is body-centered tetragonal with a space group of $P\bar{4}21C$, with lattice constants $a = b = 9.38$ Å, $c = 6.71$ Å, and an equilibrium density of 1.778 gm/cm^3.

Figure 3. Representation of the PETN molecule used in the MC simulations.

Figure 4. Resulting equilibrium configuration obtained from a spherical PETN crystal of 16 nm in diameter that was annealed for $2x10^6$ MC steps.

Figure 5. Snapshots of the simulation of deposition on a spherical PETN seed of 5 nm in diameter at 300 K. (a) initial seed and after deposition of (b) 2×10^2 molecules, (c) 2×10^3 molecules, (d) 1.5×10^4 molecules and (e) 3×10^4 molecules. The aspect ratio of the final structure (Fig. 5(e)) is approximately 7:3.

Figure 6. Comparison of the final configurations obtained after deposition of 3.5×10^4 particles on a spherical seed with (a) 5 MC steps, (b) 10 MC steps, (c) 25 MC steps, (d) 50 MC steps, and (e)

100 MC steps between particle insertion. The most elongated structure (Fig. 6(e)) has an aspect ratio of roughly 10:1.

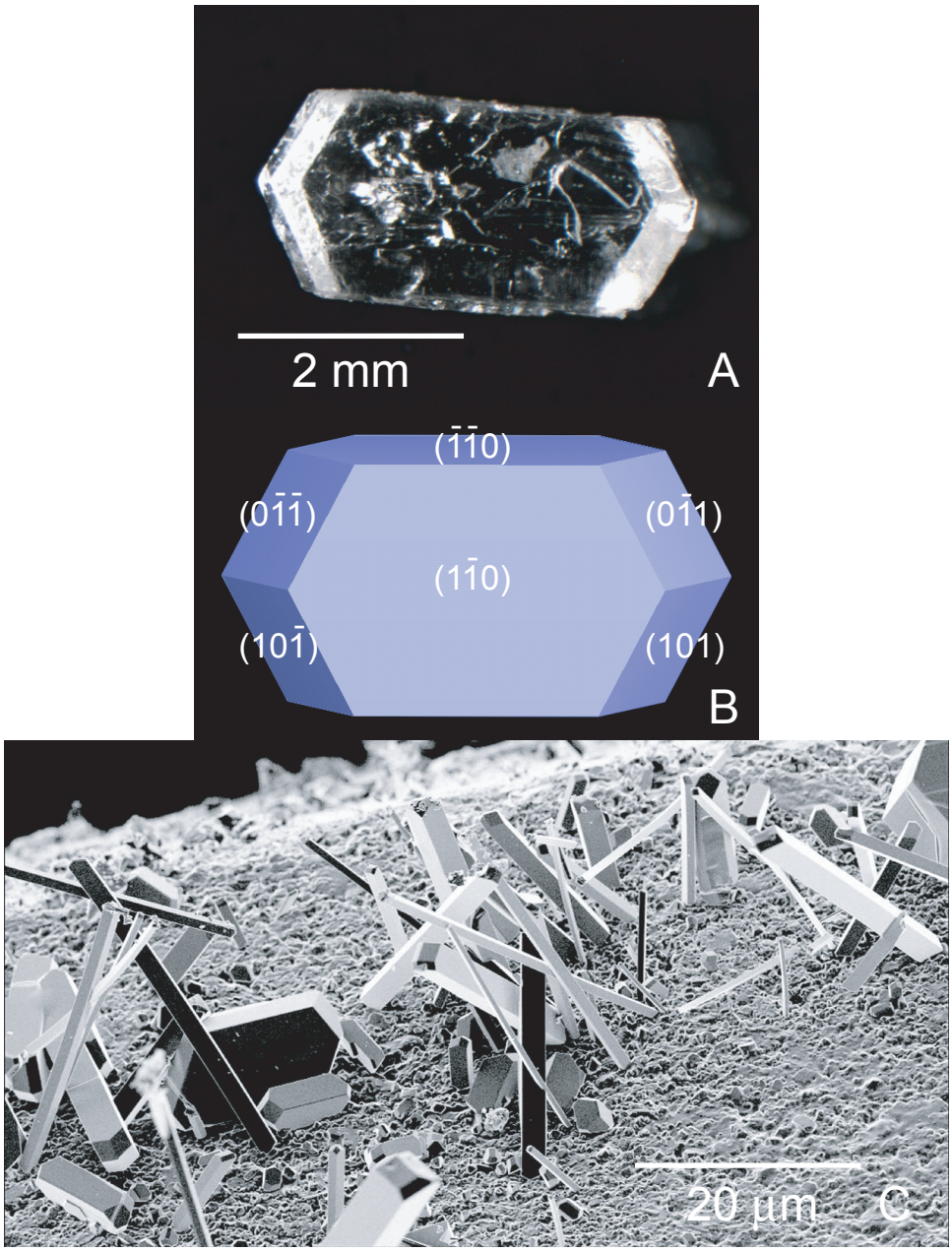

Figure 1 of 6
Zepeda-Ruiz, et al.

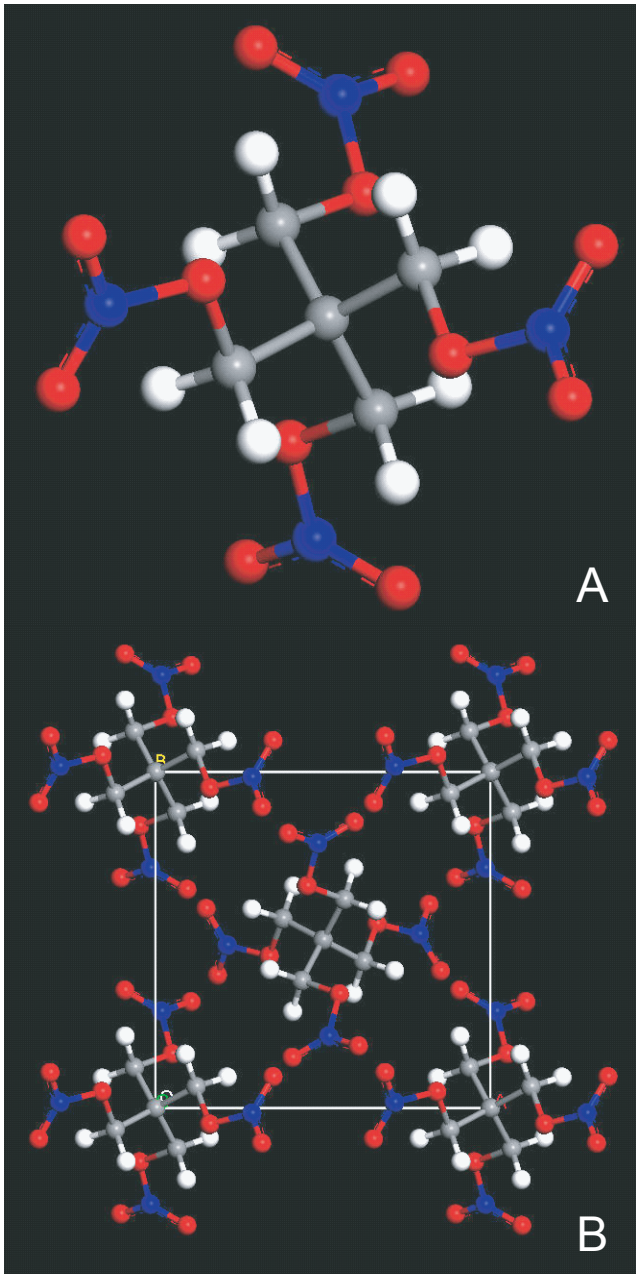

Figure 2 of 6
Zepeda-Ruiz, et al.

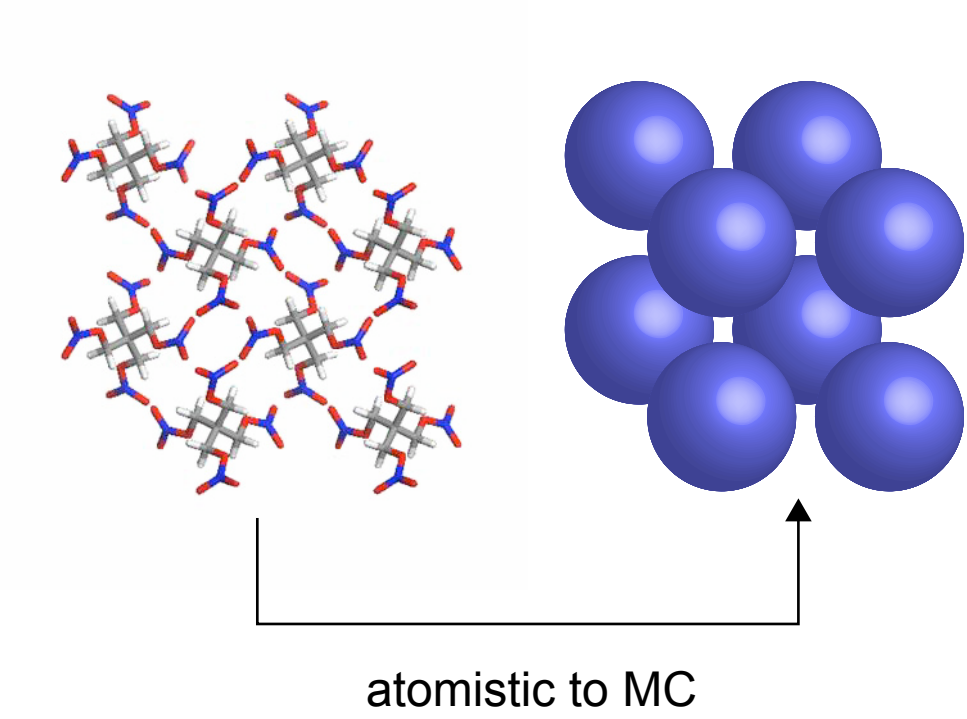

Figure 3 of 6
Zepeda-Ruiz, et al.

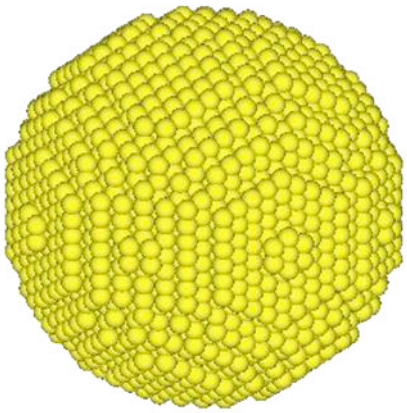

A

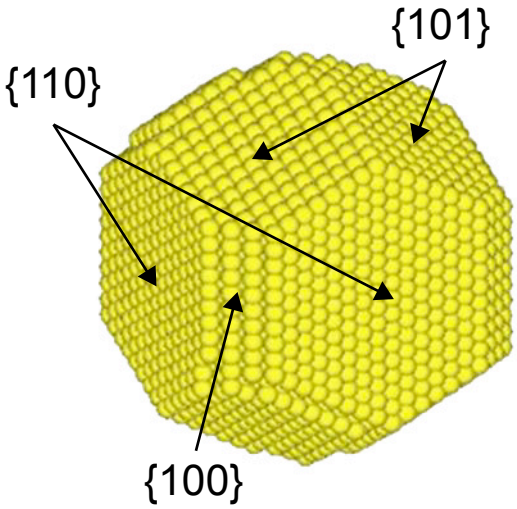

B

Figure 4 of 6
Zepeda-Ruiz, et al.

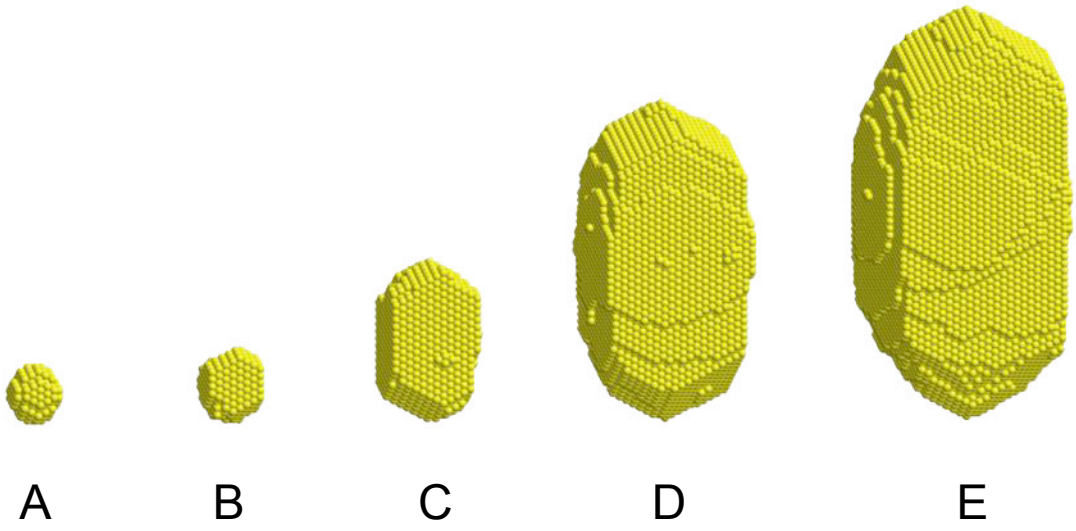

Figure 5 of 6
Zepeda-Ruiz, et al.

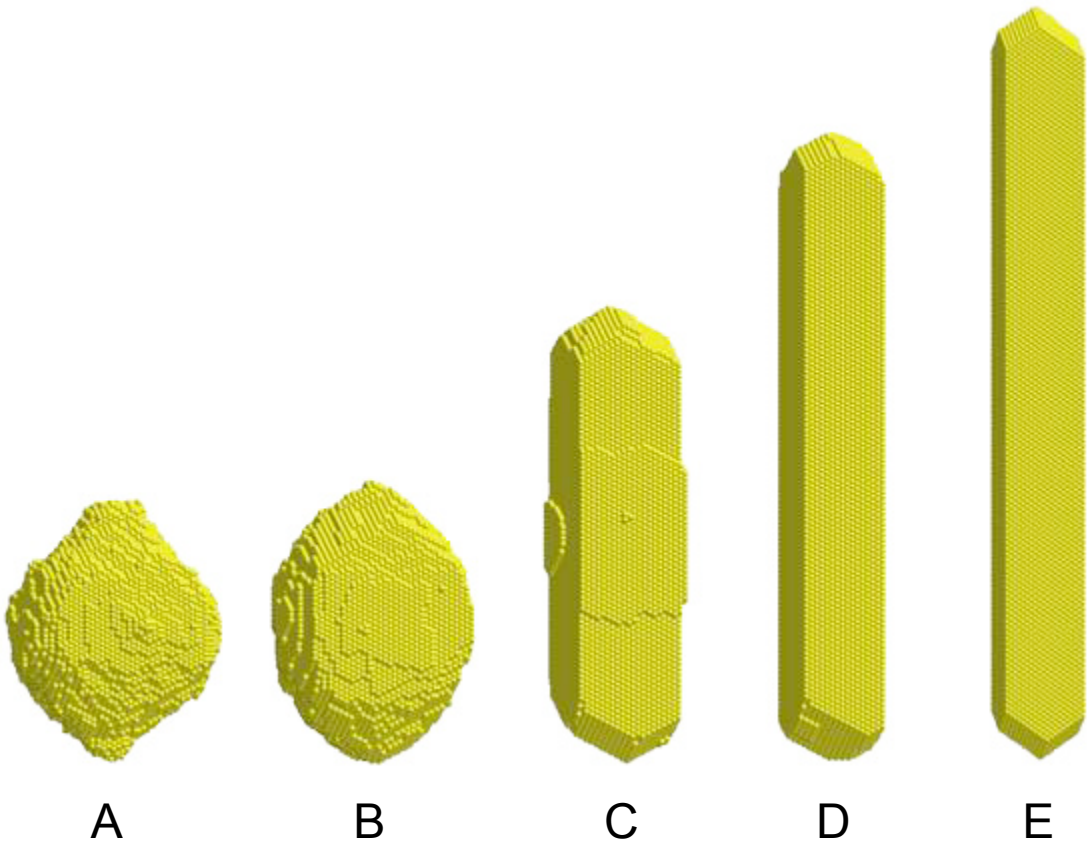

Figure 6 of 6
Zepeda-Ruiz, et al.